

Measurement of changes in optical path length and reflectivity with phase-shifting laser feedback interferometry

Ben Ovryn and James H. Andrews

The operating characteristics of a novel phase-shifting interferometer are presented. Interference arises by reflecting the light from a sample back into the cavity of a cw He-Ne laser. Changes in phase and fringe visibility are calculated from an overdetermined set of phase-shifted intensity measurements with the phase shifts being introduced with an electro-optic modulator. The interferometer is sensitive enough to measure displacements below 1 Hz with a rms error of approximately 1 nm from a sample that reflects only 3% of the 28 μW that is incident on its surface. The interferometer is applied to the determination of cantilever bending of a piezoelectric bimorph. © 1999 Optical Society of America

OCIS codes: 110.0180, 110.6880, 120.3180, 120.5050, 180.3170.

1. Introduction

There are currently a plethora of important problems that require the measurement of low-frequency changes in the optical path length (OPL) with nanometer precision. For example, in the biological sciences, Li and Schnapp recently described an interferometer with nanometer sensitivity below 10 Hz.¹ This instrument was applied in an effort to understand the nanometer-scale walking and piconewton-scale forces generated by biological micromotors.² Because of their sensitivity to misalignment, the characterization of microelectromechanical system microdevices, from microscanners to micromotors, has required the application of interferometric techniques with nanometer to micrometer precision.³ The determination of the mechanical transfer function of low-mass cantilevers that are required to operate in a 1–100-kHz bandwidth for the next generation of data storage devices has also re-

quired precise interferometric measurements.⁴ Another application that requires nanometer sensitivity at less than 100 Hz is the accurate determination of the transfer function for the pendular suspension used for the mirrors in gravitational wave interferometers.⁵

Laser feedback interferometry (LFI) demonstrates unique features that should have assured its subsequent application to a broad spectrum of disciplines since it was first exploited in the 1960's to measure changes in the OPL and the behavior of lasers.^{6–10} These features include a simple, single-axis optical arrangement that requires minimal optical components and high sensitivity at low light levels. Because the frequency selectivity of the laser, LFI is far less sensitive to incoherently reflected light than are other forms of interferometry that require all the scattered light to be collected by a photodetector. In spite of these attributes and the increased understanding of the behavior of lasers in the presence of optical feedback that has occurred in the past decade, there have been only a few uses of this method, with applications to atomic force and optical microscopy being particularly fruitful.^{11–15} To produce accurate measurements of the change in the OPL, previous LFI instruments have used a calibrated feedback loop in combination with lock-in detection to maintain an extremum of the LFI response (usually a minimum).^{11,12}

By combining the principles of phase-shifting interferometry (PSI) with LFI,¹⁵ the new instrument is not limited by the time constant associated with

B. Ovryn is with the Department of Mechanical and Aerospace Engineering, Case Western Reserve University, Cleveland, Ohio 44106 and the National Center for Microgravity Research on Fluids and Combustion, NASA Lewis Research Center, MS 110-3, 21000 Brookpark Road, Cleveland, Ohio 44135. J. H. Andrews is with the Center for Photon Induced Processes, Department of Physics and Astronomy, Youngstown State University, Youngstown, Ohio 44555.

Received 2 September 1998; revised manuscript received 4 January 1999.

0003-6935/99/101959-09\$15.00/0
© 1999 Optical Society of America

lock-in techniques, nor does it rely on a well-calibrated feedback loop to yield a measurement of the OPL. As in other applications of PSI,^{16,17} experimentally controlled phase changes are introduced, and the phase and visibility are determined independently using an overdetermined set of measurements of the intensity. Both the phase and the visibility are unaffected by the overall bias intensity. After presenting the effect of systematic and random errors, an application to the measurement of cantilever bending in a piezoelectric bimorph is presented.

2. Laser Feedback Interferometry

Although the behavior of a laser that is subjected to coherent feedback depends on the properties of the lasing medium,^{6,7,9,10,13,18} it is possible to combine PSI with LFI for the accurate determination of the phase and visibility without a deep appreciation for the underlying laser dynamics. Therefore we simplify the physics by assuming that we can model the effect of coherent feedback in a He-Ne gas laser as a three-mirror Fabry-Perot etalon, where each mirror can be represented by an intensity reflectivity R .

As we subsequently demonstrate, an adequate description of the steady-state change in the intensity of the laser that is subjected to feedback, $I(m, b, \phi)$, can be written as¹⁵

$$I(m, b, \phi) = I_0 \left[1 + m \cos(\phi) \sum_{j=0}^{\infty} (-b)^j \cos(j\phi) \right]. \quad (1)$$

Equation (1) represents the change in intensity caused by a phase difference ϕ between the incident and the reflected light with fringe visibility m . Because the laser light hits the sample and is then reflected back into the laser, the phase ϕ is related to the change in the OPL δ as $\phi = 4\pi\delta/\lambda$, where δ is given by the line integral of the index of refraction along the optical path. Also included in Eq. (1) is the effect of multiple reflections that can occur between the sample and the laser's output mirror. In LFI, the fringe visibility m and the coupling parameter b are given by

$$m = \frac{K(1 - R_2)(R_2 R_{\text{eff}})^{1/2}}{1 - R_1 + 1 - R_2} = \gamma(R_{\text{eff}})^{1/2}, \quad (2)$$

$$b = (R_2 R_{\text{eff}})^{1/2}. \quad (3)$$

Significantly, the fringe visibility is proportional to the effective amplitude reflectivity of the sample R_{eff} with the proportionality constant γ , which contains the effect of the laser's operating parameters represented by K and the mirror reflectivities R_1 and R_2 . When LFI is used in a regime where the effect of multiple reflections is small (i.e., when b is small), Eq. (1) has the same form as a two-beam interferometer. This analogy with a two-beam interferometer forms the basis for our subsequent research, and it is useful for understanding the magnitude of the fringe visibility (modulation) obtained in LFI.

The intensity that is due to the interference of two

electric fields E_1 and E_2 (which is assumed to have the same polarization) is

$$E_1 = a_1 \exp(-i\phi_1), \quad (4)$$

$$E_2 = a_2 \exp(-i\phi_2), \quad (5)$$

$$I = |E_1 + E_2|^2 = I_0[1 + m \cos(\phi)], \quad (6)$$

where $\phi = \phi_2 - \phi_1$ and the visibility is given as

$$m = 2 \frac{a_1 a_2}{a_1^2 + a_2^2}. \quad (7)$$

Because 100% of the light will not couple back into the laser, the visibility in LFI will not reach unity.

There are several possible configurations that can be used to observe laser feedback effects. In essence, the equipment consists of a laser and a photodetector and a method for reflecting the light incident on the object back into the laser cavity. The power from the laser can be monitored by dividing the beam (using a beam splitter) from the front mirror of the laser or, as in our experiments, by monitoring the power of the beam that leaves the back mirror. In this simple configuration, the interferometer can be used for fringe counting. To achieve higher accuracy and a further degree of automation, we use an electro-optic modulator situated in the beam path between the front mirror of the laser and the object. As described in Section 3, this modulator can be used to introduce discrete known changes in OPL that can be combined to solve for the phase and visibility from a least-squares solution to an overdetermined set of measurements.^{16,17}

3. Phase-Shifting Interferometry

To determine the phase ϕ and visibility m from Eq. (1), an experimentally controlled additive phase shift ψ can be introduced. Retaining only the $j = 0$ term in Eq. (1),

$$I_i(m, \phi, \psi) = I_0[1 + m \cos(\phi + \psi_i)]. \quad (8)$$

Using an overdetermined set of measurements, it is possible to solve for the three unknowns in Eq. (8) (or four depending on whether ψ is known).^{16,17} One popular algorithm, which reduces the random error in the discrete phase step ψ , uses five discrete phase shifts: $\psi = -\pi, -\pi/2, 0, \pi/2, \text{ and } \pi$.¹⁹ Once the phase step has been introduced, the intensity is measured at the corresponding phase shift. Assuming only a single reflection between the laser cavity and the sample, such that Eq. (8) is a valid representation of the steady-state intensity, then the five phase-shifted measurements can be combined, and the phase and visibility can be determined from Eqs. (9) and (10):

$$\tan(\phi) = \frac{2(I_2 - I_4)}{2I_3 - (I_1 + I_5)}, \quad (9)$$

$$m = \frac{3\{[2(I_2 - I_4)]^2 + (2I_3 - I_5 - I_1)^2\}^{1/2}}{2(I_1 + I_2 + 2I_3 + I_4 + I_5)}. \quad (10)$$

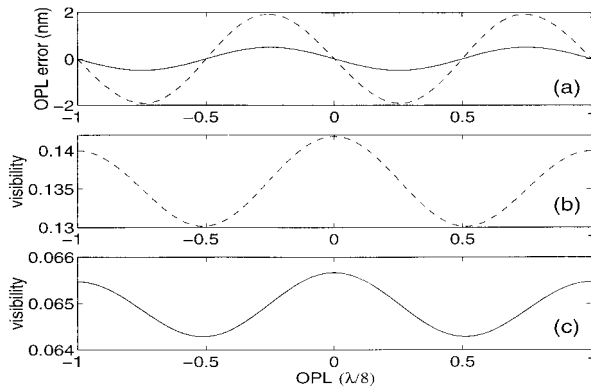


Fig. 1. (a) Error in OPL that is due to the extra reflections [Eq. (12)] calculated from the difference between the measured and the actual OPL. The visibilities shown in plots (b) and (c) represent the observed value [given by Eq. (13)] with an actual visibility equal to m . The ratio of the parameters m to b is 0.455 with $m = 0.128$ (dashed curve) or $m = 0.064$ (solid curve).

Significantly, the phase and visibility are independent of the overall bias intensity I_o . Although the visibility does not explicitly appear in the solution for the phase, the error in the estimate of the phase will increase as the visibility decreases. The errors in the estimate of the phase, caused by errors in the intensity measurements and phase shifts, have been extensively reported in the literature.^{16,17}

As more light couples back into the laser cavity (for higher-reflectivity samples, for example), the effect of multiple reflections can become significant. When Eqs. (9) and (10) are used, one additional term in Eq. (1) (i.e., $j = 1$) will not cause a phase error, but the visibility will have a systematic variation given by Eq. (11):

$$m_{j=1} = -\frac{6}{-6 + 3bm + bm \cos(2\phi)} m. \quad (11)$$

In Section 4 we show phase and visibility data that can be modeled with three additional reflections [$j = 3$ in Eq. (1)]. In this case, the measured phase $\phi_{j=3,4}$ is related to the actual phase by Eq. (12):

$$\tan(\phi_{j=3,4}) = \frac{1 - b^2 \cos(2\phi) + b^4 \cos(4\phi)}{1 + b^2 \cos(2\phi) + b^4 \cos(4\phi)} \tan(\phi). \quad (12)$$

For three reflections, the observed visibility is related to the actual visibility m by Eq. (13):

$$m_{j=3} = \frac{-3\sqrt{2} m [2 + 2b^2 + b^4 + b^2(2 + b^2)\cos(4\phi)]^{1/2}}{-6 + 3bm + (b + b^3)m \cos(2\phi) + 3b^3 m \cos(4\phi)}. \quad (13)$$

The systematic errors in the phase and visibility caused by extra reflections [Eqs. (11)–(13)] are unique to the algorithms used to determine the phase and visibility [Eqs. (9) and (10)]. Figure 1 shows the

error in the phase and visibility for two ratios of the visibility to the coupling parameter m/b equal to 0.455 with $m = 0.128$ and $m = 0.064$. The OPL error [Fig. 1(a)] is calculated from the difference between the measured and the actual OPL from Eq. (12). The visibility plots represent the observed value [given by Eq. (13)] with an actual visibility $m = 0.128$ and $m = 0.064$ [Fig. 1(b) and (c)], respectively.

4. Experimental Calibration of the Instrument and Determination of Random and Systematic Errors

We performed a series of experiments to verify the applicability of PSI for the determination of the phase and visibility in LFI, to quantify the effects of systematic and random errors, and to determine the step response of the interferometer. A phase-shifting laser feedback interferometer was assembled from a He–Ne laser (Uniphase, 1107P). The beam emitted from the front of the laser was sent through an electro-optic modulator (EOM) (New Focus, 4002), a linear polarizer with a fixed orientation parallel to the polarization of the laser, and then focused onto a sample using a $50\times/0.42$ N.A. long working distance microscope objective (Mitutoyo, G Plan NIR). Fluctuations in the laser's steady-state power were determined by monitoring the light transmitted through the laser's rear mirror using a photodetector (New Focus, 2001). The voltage signal from the photodetector was digitized with a 100-kHz, 16-bit analog-to-digital board on a PC bus (Keithley, DAS 1800 HR); this board was also used to send voltage steps to a high-voltage operational amplifier (New Focus, 3211) and then to the EOM. The process was automated with LabView (National Instruments). The entire apparatus was mounted on a vibration isolation table and enclosed in a double Plexiglas box.

Because our five-phase-shift algorithm requires equal shifts separated by $\pi/2$, it is initially important to determine the correct voltage to be sent to the EOM. We determined the modulation depth for the EOM and amplifier combination by first calibrating the gain of the amplifier and then monitoring the photodetector signal with an oscilloscope and determining the voltage required to sweep through one fringe. We obtained a modulation depth of 61 mrad/V for the EOM and a gain of 41.6 V/V for the amplifier; this corresponds to a change of 0.3 nm/mV applied to the amplifier. We also used the phase-shifting algorithm to verify the $\pi/2$ phase step.^{16,17}

A. Step Response of the Interferometer to Phase Shifts

We examined the step response of the interferometer by applying a series of discrete voltage steps to the EOM. The voltage from the photodetector was digitized with a fast oscilloscope; for this experiment, a small silicon wafer was held fixed at the focus of the objective. Figure 2 shows two sets of five voltage steps to the EOM and the output of the photodetector. At each voltage step, the phase was maintained for a controlled interval that was typically used to average 100 intensity measurements.

Figure 2 indicates that the time for five phase

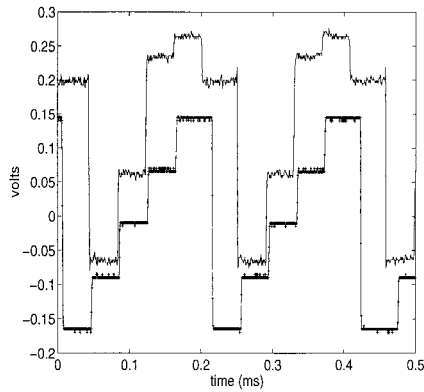


Fig. 2. Step response of the interferometer (top trace) to two sets of five sequential voltage steps to the EOM (bottom trace). Each set of five phase shifts is required for a single phase measurement.

shifts, including the controlled interval maintained at each phase shift, is approximately 200 μ s; by reducing the interval it would be possible to collect all five phase shifts in a significantly shorter interval. The time required to introduce the phase shifts and collect the data is a small fraction of the total time required for an on-line calculation and display of the phase and visibility; the total sampling time per phase measurement was approximately 50 ms. Although this method is not nearly as fast as a post-collection data analysis (in which the phase-shifted intensity measurements are written to RAM or disk), the visual feedback of an on-screen display of the phase and visibility provides useful information. The time required for a single phase measurement limits the maximum slope (amplitude and periodicity) of the phase change that can be measured without aliasing.

We verified that the temporal response of the laser does not distort the applied phase shifts. We measured the magnitude and phase of the signal from the photodetector when 400-, 800-, or 1000-kHz sinusoids from a function generator were applied to the EOM. Figure 3 shows a flat frequency response at (a) 400 kHz, (b) a phase shift at 800 kHz, and (c) both magnitude and phase distortion at 1 MHz.

B. Systematic Error that is Due to Multiple Reflections

To vary the amount of light that was reflected from a sample back into the laser, the previous experimental setup was modified by the insertion of various neutral density (ND) filters between the laser and the EOM. A 1.15-V linear ramp was applied to the EOM using a function generator that corresponds to a change in the OPL of 147 nm (approximately $\lambda/4$). The EOM was also used to measure simultaneously the OPL and the visibility by superposing the five phase shifts on the voltage ramp using a summing voltage amplifier (New Focus, 3211).

Figure 4 shows the measured change in the OPL obtained at a mean visibility of $m = 0.136$. In Fig. 4(a) the OPL, plotted as a function of time, indicates total change in OPL of 146 nm; however, oscillations

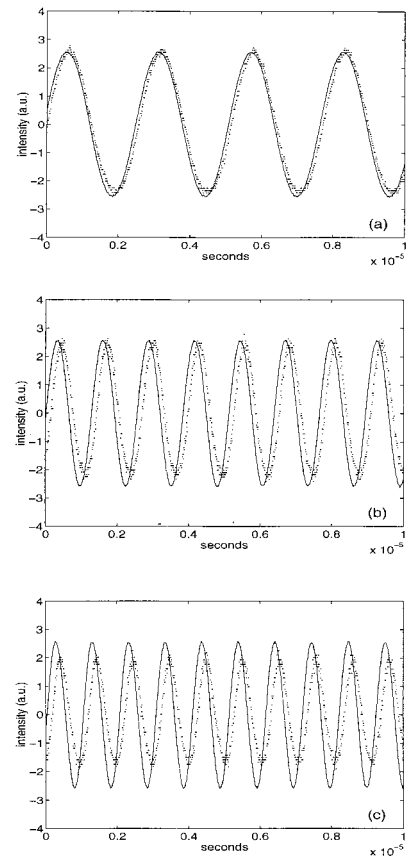


Fig. 3. Laser intensity when a sinusoidal voltage of (a) 400 kHz, (b) 800 kHz, and (c) 1 MHz was applied to the EOM. Solid curve (time domain) represents the input voltage to the EOM.

can be observed on the ramp. To highlight the dependence of the measured OPL and visibility on the applied linear change in OPL, the subsequent plots [Fig. 4(b), 4(c), and 4(d)] are shown as a function of the OPL normalized with respect to the wavelength. Both the visibility and the OPL demonstrate a periodic variation; the oscillations in the OPL become clear when a least-squares line is subtracted from the measured OPL [Fig. 4(c)]. Also shown [solid curves in Fig. 4(b) and 4(c)] is the result of a simultaneous nonlinear least-squares fit to these data sets using Eqs. (12) and (13) with a visibility $m = 0.128$ and coupling constant $b = 0.282$. As indicated in Fig. 4(c) the oscillations that are due to the multiple reflections lead to a systematic deviation of the measured OPL from the applied linear ramp of ± 2 nm. After subtracting the predicted oscillations from the raw OPL data [Fig. 4(d)], however, the systematic error is considerably reduced, although not eliminated, and the random error in the data is revealed; the rms error is 0.15 nm.

C. Systematic Errors Caused by Environmental Phase Drift

Figure 5 shows the change in OPL and visibility measured during a 50-s period with the sample held fixed and without applying an additional phase ramp to

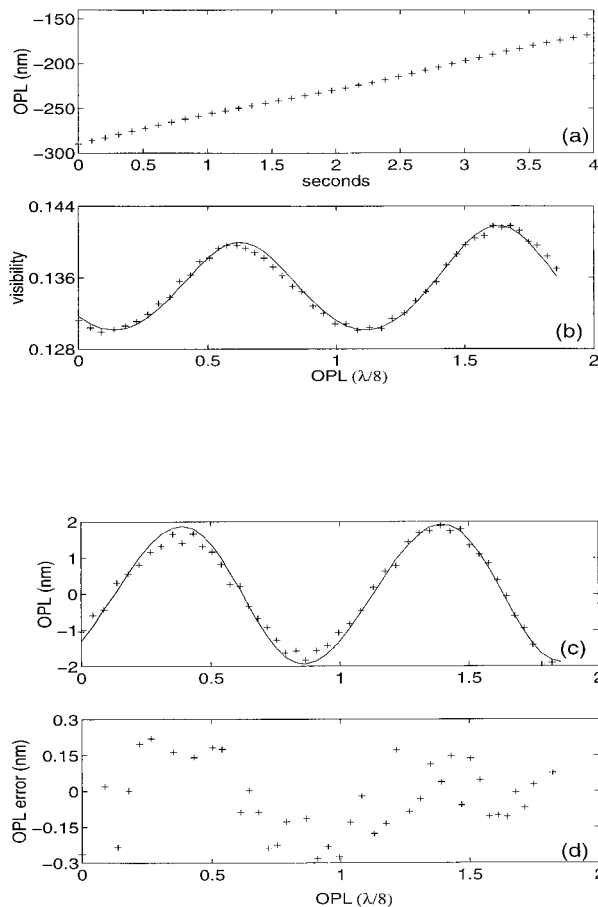


Fig. 4. (a) OPL and (b) visibility measurements obtained at moderately high visibility. Both the visibility and the OPL show systematic oscillations that depend on the value of the OPL. The solid curves in (b) and (c) represent fits using Eqs. (12) and (13) with $m = 0.128$ and $b = 0.282$.

the EOM. It can be observed that there is low-frequency systematic drift in the OPL, with an essentially linear drift during the last 30 s of the data set. An estimate of the random error in this measurement

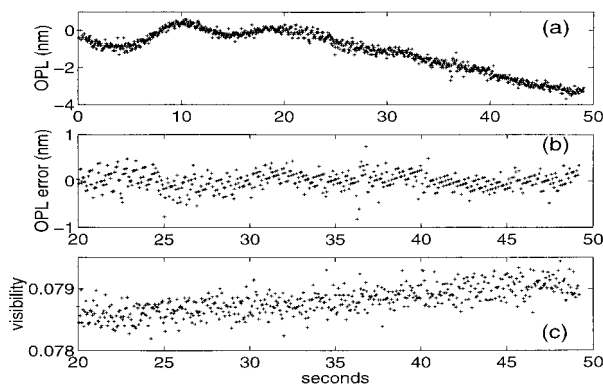


Fig. 5. Low-frequency systematic variation in the OPL (a) caused by environmental perturbations during a 50-s period; (b) the rms error in the OPL calculated from a linear fit to the last 30 s of data; and (c) visibility during the 30-s period.

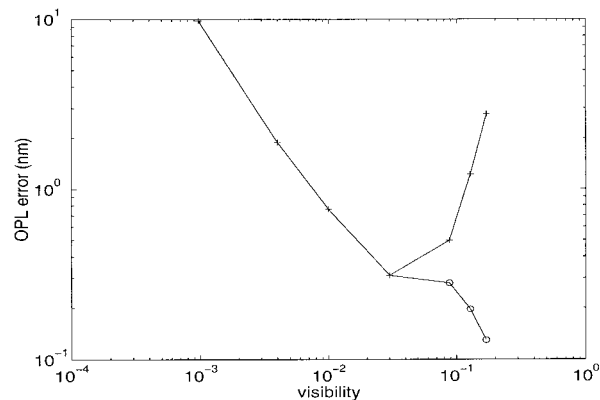


Fig. 6. Error in the measured OPL as a function of the visibility. The crosses represent the raw data, and the circles represent the data corrected for the effect of multiple reflections.

is obtained by subtracting a least-squares line from this linear portion of the curve [Fig. 5(b)]. A histogram of the data shows a Gaussian distribution with a rms error in OPL of 0.18 nm. A small amount of systematic drift is still present in this estimate [Fig. 5(b) and 5(c)]. Although the data in Fig. 5 are representative, the drift in the OPL will vary depending on recent perturbations to the system.²⁰ Under quiescent conditions, we observed fluctuations in the OPL of less than ± 5 nm during a 5-min period.

D. Random Errors

A measurement was made of the variation of the random error in the OPL as a function of the amount of optical power reflected by the sample. Seven ND filters with optical densities (OD's) of 0.1, 0.3, 0.5, 1.0, 1.5, 2.0, and 2.5 were used to attenuate the power from the laser. Before attenuation, the power measured at the sample was 0.9 mW. Using the same voltage ramp to the EOM as just described, we calculated the rms error in the determination of OPL by subtracting a least-squares line from a measurement of a single ramp. The resulting rms error in OPL is shown as a function of the measured visibility in Fig. 6. At small visibilities, the error is observed to increase as the visibility decreases. At large visibility, however, the error becomes biased and increases. After modeling the effect of the multiple reflections, it is possible to reduce the bias (circles in Fig. 6), and the error is observed to decrease at higher visibilities. Because the systematic error is not removed completely, the calculated error is biased by some residual systematic error. Without correcting for the systematic error, the error in OPL has a minimum value of approximately 0.31 nm obtained at a visibility of 0.03. After correction using Eq. (12), the minimum error in the OPL measurement decreases to approximately 0.13 nm at a visibility of 0.17.

Figure 7 shows a plot of the visibility as a function of transmitted intensity T corresponding to the OD of the ND filter. For example, when the OD is 2, only 1 part in 10^4 of the incident power is reflected back through the ND filter, corresponding to an ampli-

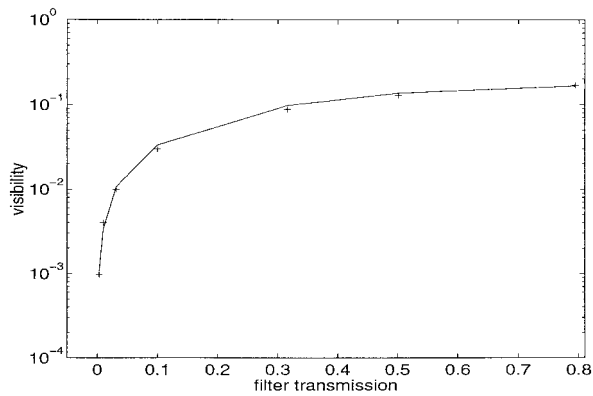


Fig. 7. Visibility as a function of the transmission of the ND filter. At high visibility, the data were corrected for systematic errors that were due to multiple reflections. The solid curve is based on Eq. (7).

tude reflectivity of 1% and a measured visibility $m = 0.0042$. At this OD, $9 \mu\text{W}$ were incident on the sample with a maximum of $0.09 \mu\text{W}$ coupled back into the laser. Also shown (solid curve) is the predicted visibility based on Eq. (7), with $a_1 = Ta_2$, where a_2 represents the amplitude of the field in the laser, and a_1 represents the field on the sample; the calculated visibility m is normalized to the maximum measured visibility.

For small changes in OPL, the systematic error that dominates the total error at higher visibility can be small. As indicated in Fig. 1, the magnitude of this error depends on the absolute value of the OPL, with a minimum obtained at intervals of $n\lambda/16$; alternatively, the rate of change of the error is smallest at $(2n + 1)\lambda/32$, with integer n . Figure 8 shows the measured OPL and visibility when a 40-mV linear ramp was applied to the EOM; a mean value of 165 nm was subtracted from the data. The rms error in OPL [Fig. 8(c)] at a visibility of 0.078, calculated over the 5-nm ramp, was 0.14 nm. Figure 9 shows the OPL and visibility that are due to the same magnitude voltage ramp, but obtained at a higher visibility. Systematic drift is evident in the 40 s of collection

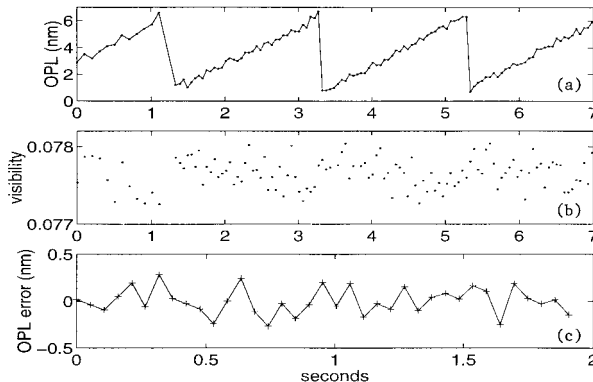


Fig. 8. Measured OPL and visibility for a 5-nm ramp applied to the EOM. The rms OPL error, obtained from a linear fit to a single period, is 0.14 nm.

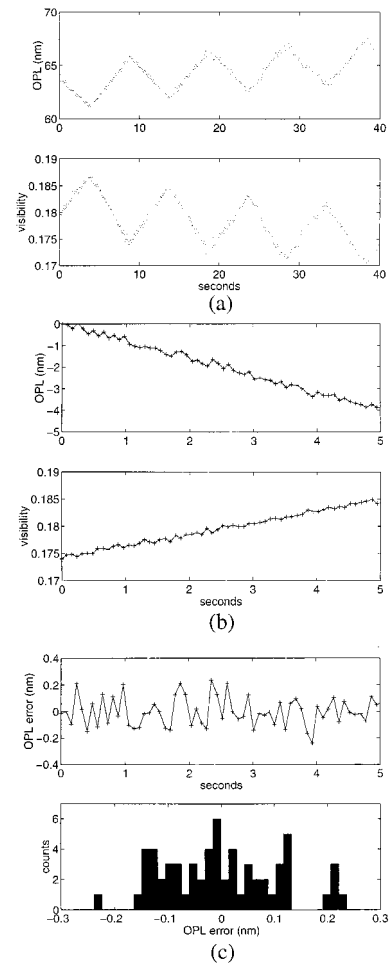


Fig. 9. Linear change in OPL that is due to a 40-mV voltage ramp applied to the EOM. (a) The presence of a linear drift in the OPL during the 40 s is evident. (b) Variation in OPL and visibility during a 5-s period. (c) The rms error in OPL, obtained from a linear fit to the data, is 0.13 nm; a histogram indicates the error distribution.

[Fig. 9(a)]. The data from one period of the ramp [Fig. 9(b)] shows that the variation of the visibility is linear, indicating that the effect of multiple reflections has a linear dependence on OPL. The rms phase error, obtained from a least-squares linear fit, is 0.13 nm [Fig. 9(c)]; a histogram of the errors indicates a multimodal distribution, representing both the random and the residual systematic errors. The systematic error with $m = 0.17$ and $b = m/0.455$ is given by Eq. (12) to be 0.086 nm.

Figure 10 shows a sinusoidal oscillation of the OPL caused by sinusoidal voltage input to the EOM. The resulting 2-nm change in OPL is discerned, and the absence of systematic oscillations in the visibility indicates that the effect of multiple reflections are negligible. For comparison, Fig. 11 shows a larger change in OPL, caused by a mechanical translation of the sample using a piezoelectric translator (Queensgate, S100), obtained at the same visibility. In this

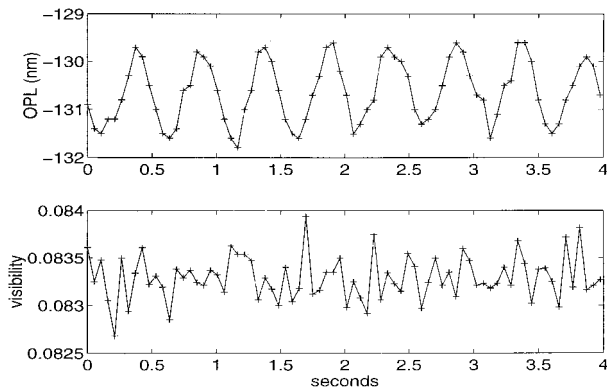


Fig. 10. Small sinusoidal change in the OPL that is due to a sinusoidal voltage applied to the EOM. The visibility is essentially flat, indicating the absence of systematic errors.

case, the EOM was used solely for phase shifting. Oscillations in the visibility are significant.

E. Effect of Averaging on Reducing the Random Errors

When the visibility is low enough that the systematic errors are small, then it may be possible to decrease the error in the measurement of the OPL by averaging over repeated phase measurements.²⁰ Figure 12

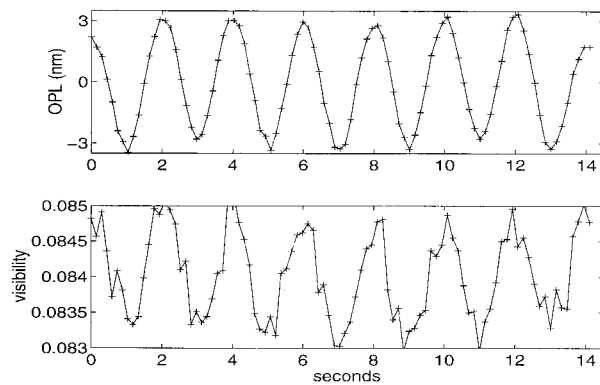


Fig. 11. Sinusoidal change in the OPL that is due to a sinusoidal voltage applied to a piezoelectric translator that is moving parallel to the optical axis.

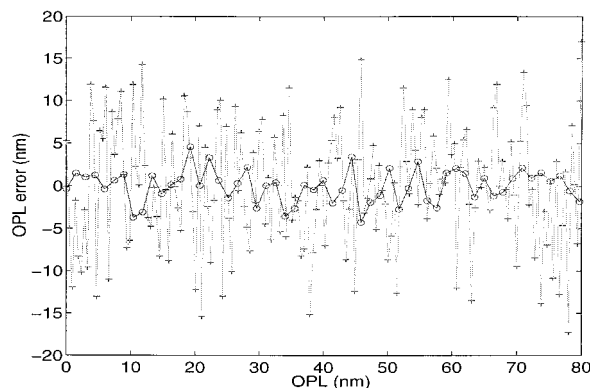


Fig. 12. Reduction in error in OPL by averaging ten phase measurements; the error was reduced from approximately 7 to 2.2 nm.

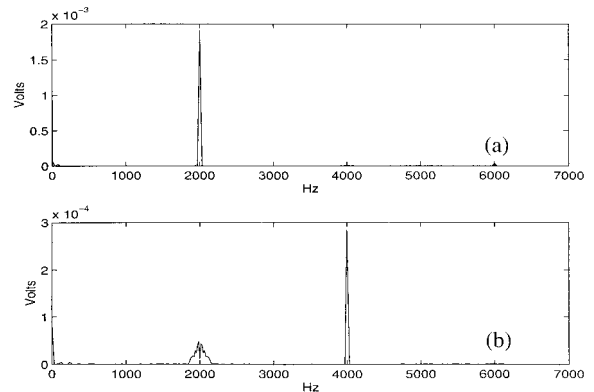


Fig. 13. Photodetector signal from the spectrum analyzer when the EOM was modulated at 2 kHz. The first harmonic was maximized (a) by changing the dc offset ϕ_{dc} , whereas there is residual first-harmonic response in (b) the nearly maximal second harmonic.

shows the rms error in the OPL before and after averaging ten phase measurements. The rms error was determined from a linear fit to an applied phase ramp at a visibility of $m = 0.0047$. The error in the OPL was reduced from 7.1 to 2.2 nm, corresponding an improvement of $\sqrt{10}$.

5. Harmonic Response of the Interferometer

When the change in OPL has a sinusoidal as well as a dc component, the measured intensity will have both dc and ac components, given by Eq. (8) (with $\psi = 0$) and $\phi = \phi_{dc} + \phi_{ac} \sin(\omega t)$:

$$I_{dc}(m, \phi) = I_0 [1 + m \cos(\phi_{dc}) J_0(\phi_{ac})], \quad (14)$$

$$I_{ac}(m, \phi, \omega) = I_0 \left\{ 2m \cos(\phi_{dc}) \sum_{n=1}^{\infty} J_{2n}(\phi_{ac}) \times \cos(2n\omega t) - 2m \sin(\phi_{dc}) \times \sum_{n=1}^{\infty} J_{2n-1}(\phi_{ac}) \sin[(2n-1)\omega t] \right\}. \quad (15)$$

According to Eqs. (14) and (15) the dc response will be reduced by the presence of the ac component, and the ac component will have a response at the fundamental frequency as well as harmonics. Because the Bessel functions of a given argument become progressively smaller at higher orders, the strength of the overtones will become progressively weaker. It can also be observed that the even and odd harmonics have a quadrature dependence on the dc component of the phase.

To verify that the interferometer responds in accordance with Eq. (15), we applied a 2-kHz sinusoidal oscillation to the EOM (with the sample held fixed). Figure 13 shows the spectral response (Stanford Research Systems, 770) of the photodetector signal. Initially, ϕ_{dc} was varied to minimize the second harmonic [Fig. 13(a)], then the second harmonic [Fig. 13(b)] was nearly maximized (there is some residual

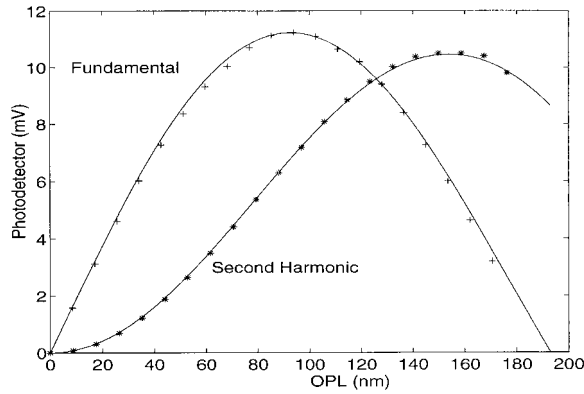


Fig. 14. LFI response at the fundamental and second harmonic as a function of the amplitude of the ac oscillation of the EOM. The solid curves represent fits to the harmonics based on the first and second Bessel functions.

first harmonic). By measuring the maximum magnitude of the fundamental as a function of ϕ_{ac} and then subsequently maximizing the second harmonic, we verified the Bessel function dependence (Fig. 14).

According to Eq. (15) it is possible to determine either dc or sinusoidal changes in the OPL based on a measurement of I_{ac} . For example, there are several alternative methods for determining ϕ_{dc} . One method is to obtain ϕ_{dc} from a ratio of the first two harmonics:

$$\tan(\phi_{dc}) = -\frac{J_2(\phi_{ac}) I_{ac}(\omega)}{J_1(\phi_{ac}) I_{ac}(2\omega)}. \quad (16)$$

This measurement requires a determination of the ratio of the two Bessel functions at ϕ_{ac} .

It is also possible to measure the dc component of the OPL by introducing an equal but opposite change in OPL (with a feedback loop, for example) so as to null one of the harmonics. This method was exploited by Bearden *et al.* in their laser feedback microscope.¹¹

Phase-shifting techniques can also be applied on top of the ac carrier, to make a determination of ϕ_{dc} , by monitoring just the second harmonic, for example. The presence of $J_2(\phi_{ac})$ in the second-harmonic response will affect a determination of the visibility, but not the OPL. This approach has the added advantage of reducing the $1/f$ noise compared with the dc version of the PSI and the LFI.

6. Measurement of Cantilever Bending of a Piezoelectric Bimorph

To verify the accuracy of the phase-shift method as applied to LFI, we measured the cantilever bending of a piezoelectric bimorph. The piezoelectric bimorph is a sandwich of two piezoelectric elements with equal and opposite piezoelectric coefficients d_{31} ; these elements are separated by an insulator (we neglect the thickness of this layer). The surfaces of the bimorph (width b) are covered with (silver) electrodes.

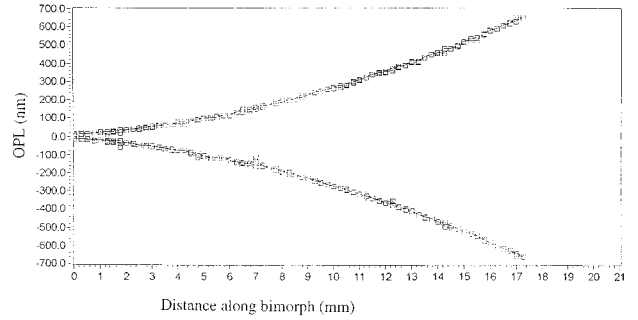


Fig. 15. Bending curves for the bimorph when ± 2.000 V were applied to the bimorph; there is no directional ambiguity in the displacement measurement. The multiple data points at each of the $250 \mu\text{m}$ increments are caused by superimposing the displacement measured in both directions of the scan, with the first scan beginning at the base of the bimorph (we corrected for the 2π ambiguity for the first data point acquired on the retrace).

When a voltage difference is applied across the electrodes separated by a distance h , a stress develops in each half of the bimorph, with one half of the bimorph in tension and the other in compression. The net bending moment is given by

$$M_0 = \sigma_{11} h^2 \frac{b}{4}, \quad (17)$$

and the stress is given by

$$\sigma_{11} = d_{31} Y E_3, \quad (18)$$

where Y is the Young's modulus of the material and E_3 is the field applied across the bimorph. The deflection of the beam u_3 , with moment of inertia I , at a distance u_1 from the base of the beam is

$$u_3 = -\frac{M_0}{2YI} u_1^2 = -\frac{3}{2} \frac{d_{31} \Delta V}{h^2} u_1^2. \quad (19)$$

According to Eq. (19) the bending of the bimorph is proportional to the applied voltage, inversely proportional to the square of the thickness of the sandwich, varies quadratically with the distance from the clamped end of the bimorph, and is independent of the Young's modulus of the material.

To measure the bending of the bimorph as a function of the distance from the base of the clamp, the bimorph (Vernitron, PZT-5H) was mounted so that it formed a cantilever beam with dimensions $12.5 \text{ mm} \times 21 \text{ mm} \times 0.64 \text{ mm}$. The clamp was attached to a uniaxial translation stage (Klinger, UT 100) that operated under closed-loop control.

The bimorph was positioned at the focus of the long working distance objective used previously, and the clamp and bimorph were translated in $250 \mu\text{m}$ increments perpendicular to the focused beam. At each location, two measurements of the OPL were made, one before and another immediately after applying a voltage to the bimorph with the difference representing the net displacement. Figure 15 shows the measured bending when two voltages (± 2.000 V) were

sequentially applied across the bimorph. Because the total displacement was larger than one fringe, the data had to be phase unwrapped. The data indicate that there was no directional ambiguity in the phase measurement when the sign of the applied voltage changed with the negative displacement indicating bending toward the laser. The multiple data points at each location on the bimorph are caused by superimposing the displacement measured in two directions of the scan, with the first scan beginning at the base of the bimorph. After a 17-mm scan, the direction of the scan was reversed, and we corrected for the 2π ambiguity for the first data point acquired on the retrace. The good agreement obtained between the displacements acquired at each location demonstrates the repeatability of the measurement. Furthermore, the piezoelectric coefficient for the material determined from a quadratic fit to the data was in agreement with measurements (for the same bimorph) using the harmonic response of the interferometer²⁰ and with those based on real-time phase-shifted holographic interferometry (324 ± 16 pm/V)^{21,22} and the manufacturer's specification (274 ± 55 pm/V).

7. Conclusions

We have designed a phase-shifting laser feedback interferometer that can be used to measure oscillatory and dc changes in the OPL. Response times are limited by photon lifetime, detector electronics, and modulator rise time rather than lock-in detection and feedback loop parameters. Changes in the OPL can be determined with subnanometer accuracy below 1 Hz. The accuracy of the instrument has been verified with the measurement of cantilever bending of a bimorph. We have also verified the predicted systematic errors caused by multiple reflections at higher visibility. A further attribute of the method is that high signal-to-noise ratios can be achieved with low-power deposition on the sample.

The authors gratefully acknowledge David G. Fischer, National Center for Microgravity Research on Fluids and Combustion, for a critical reading of the manuscript. This research was supported by the Advanced Technology Development Program of the Microgravity Research Division, NASA.

References

1. D. Li and B. J. Schnapp, "Improved nm displacement detector for microscopic beads at frequencies below 10 Hz," *Rev. Sci. Instrum.* **68**, 2195–2199 (1997).
2. K. Svoboda, C. F. Schmidt, B. J. Schnapp, and S. M. Block, "Direct observation of kinesin stepping by optical trapping interferometry," *Nature (London)* **365**, 721–727 (1993).
3. M. H. Kiang, O. Solgaard, K. Y. Lau, and R. S. Muller, "Electrostatic combdrive-actuated micromirrors for laser-beam scanning and positioning," *IEEE J. Microelectromech. Syst.* **7**, 27–37 (1998).
4. B. Chui, W. T. D. Stowe, Y. Sungtack, K. E. Goodson, T. W. Kenny, H. J. Mamin, B. D. Terris, R. P. Ried, and D. Rugar, "Low-stiffness silicon cantilevers with integrated heaters and piezoresistive sensors for high density AFM thermomechanical data storage," *IEEE J. Microelectromech. Syst.* **7**, 69–78 (1998).
5. E. Calloni, L. D. Fiore, A. Grado, and L. Milano, "An interferometric device to measure the mechanical transfer function of the VIRGO mirror suspensions," *Rev. Sci. Instrum.* **69**, 1882–1885 (1998).
6. Th. H. Peek, P. T. Bolwijn, and C. Th. Alkemade, "Axial mode number of gas lasers from moving-mirror experiments," *Am. J. Phys.* **35**, 820–831 (1967).
7. E. B. Hooper, Jr., and G. Bekefi, "Laser interferometer for repetitively pulsed plasmas," *J. Appl. Phys.* **37**, 4083–4094 (1966); erratum, **38**, 1998 (1967).
8. P. T. Bolwijn, "Single mode tuning dip in the modulated power output of gas lasers," *Phys. Lett.* **19**, 384–385 (1963).
9. R. Lang and K. Kobayashi, "External optical feedback effects on semiconductor injection laser properties," *IEEE J. Quantum Electron.* **QE-16**, 347–355 (1980).
10. G. A. Acket, D. Lenstra, A. J. Den Boef, and B. H. Verbeek, "The influence of feedback intensity on longitudinal mode properties and optical noise in index-guided semiconductor lasers," *IEEE J. Quantum Electron.* **QE-20**, 1163–1169 (1984).
11. A. Bearden, M. P. O'Neill, L. C. Osborne, and T. L. Wong, "Imaging and vibrational analysis with laser-feedback interferometry," *Opt. Lett.* **18**, 238–240 (1993).
12. R. Juskaitis, T. Wilson, and N. P. Rea, "Compact confocal interference microscopy," *Opt. Commun.* **109**, 167–177 (1994).
13. D. Sarid, V. Weissenberger, D. A. Iams, and J. T. Ingle, "Theory of the laser diode interaction in scanning force microscopy," *IEEE J. Quantum Electron.* **25**, 1968–1972 (1989).
14. D. Sarid, D. A. Iams, J. T. Ingle, and V. Weissenberger, "Performance of a scanning force microscope using a laser diode," *J. Vac. Sci. Technol. A* **8**, 378–383 (1990).
15. B. Ovryn and J. H. Andrews, "Phase-shifted laser feedback interferometry," *Opt. Lett.* **23**, 1078–1080 (1998).
16. K. Creath, "Phase measurement interferometry techniques" in *Progress in Optics XXVI*, E. Wolf, ed. (North-Holland, Amsterdam, 1988), pp. 349–393.
17. J. E. Greivenkamp and J. H. Bruning, "Phase shifting interferometry" in *Optical Shop Testing*, D. Malacara, ed. (Wiley, New York, 1992), pp. 501–598.
18. A. Yariv, *Quantum Electronics* (Wiley, New York, 1989), p. 192ff.
19. P. Hariharan, B. F. Oreb, and T. Eiju, "Digital phase-shifting interferometry: a simple error-compensating phase calculation algorithm," *Appl. Opt.* **26**, 2504–2505 (1987).
20. B. Ovryn, J. H. Andrews, S. J. Eppell, and J. D. Khaydarov, "Phase shifted real time laser feedback interferometry," in *Laser Interferometry VIII: Techniques and Analysis*, M. Kujawinska, R. J. Pryputniewicz, and M. Takada, ed., *Proc. SPIE* **2860**, 263–274 (1996).
21. B. Ovryn and E. M. Haacke, "Temporal averaging of phase measurements in the presence of spurious phase drift: application to phase-stepped, real-time holographic interferometry," *Appl. Opt.* **32**, 147–154 (1993).
22. B. Ovryn, "Two camera phase measurements using phase stepped, real-time holographic interferometry," in *Holography, Interferometry and Optical Pattern Recognition in Biomedicine III*, H. Podbielska, ed., *Proc. SPIE* **1889**, 120–131 (1993).